JACS
JOURNAL OF THE AMERICAN CHEMICAL SOCIETY
pubs.acs.org/JACS
Article

Engineering DNA-Functionalized Nanostructures to Bind Nucleic Acid Targets Heteromultivalently with Enhanced Avidity

Brendan R. Deal, Rong Ma, Victor Pui-Yan Ma, Hanquan Su, James T. Kindt, and Khalid Salaita*

Cite This: https://dx.doi.org/10.1021/jacs.0c01568
Read Online

ABSTRACT: Improving the affinity of nucleic acids to their complements is an important goal for many fields spanning from genomics to antisense therapy and diagnostics. One potential approach to achieving this goal is to use multivalent binding, which often boosts the affinity between ligands and receptors, as exemplified by virus−cell binding and antibody−antigen interactions. Herein, we investigate the binding of heteromultivalent DNA−nanoparticle conjugates, where multiple unique oligonucleotides displayed on a nanoparticle form a multivalent complex with a long DNA target containing the complementary sequences. By developing a strategy to spatially pattern oligonucleotides on a nanoparticle, we demonstrate that the molecular organization of heteromultivalent nanostructures is critical for effective binding; patterned particles have a ∼23 order-of-magnitude improvement in affinity compared to chemically identical particles patterned incorrectly. We envision that nanostructures presenting spatially patterned heteromultivalent DNA will offer important biomedical applications given the utility of DNA-functionalized nanostructures in diagnostics and therapeutics.

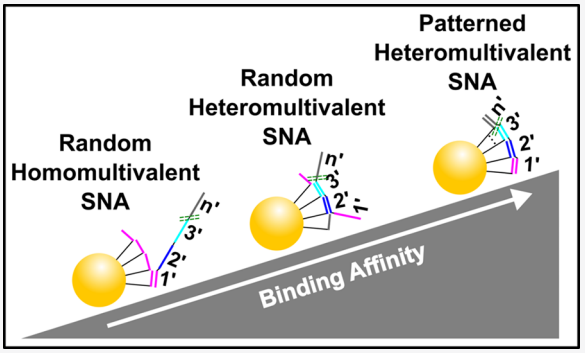

INTRODUCTION

A multivalent interaction occurs when a multivalent ligand binds a multivalent receptor through several individual ligand−receptor pairs.[1] Such interactions commonly offer an enhanced collective affinity, or avidity, and thus, Nature has evolved to utilize multivalent interactions to aid in many biological and chemical processes. For example, uptake of influenza viral particles into cells is aided by the avid multivalent interaction between a trivalent hemagglutinin molecule and multiple sialic acid molecules on the cell membrane.[2] Inspired by such natural multivalent interactions, many synthetic multivalent interactions have been engineered to tightly bind a receptor, such as a peptide or a viral particle, for improved sensing and therapeutics.[3,4] An especially noteworthy example of a multivalent binding interaction utilized both naturally and synthetically is nucleic acid hybridization. Polynucleotide hybridization occurs through two distinct levels of multivalent binding. The primary level of multivalent binding is the 2−3 hydrogen bonds formed between each nucleobase pair, whereas the secondary level is the concurrent base stacking and binding of a series of nucleobases to their complementary bases on another polynucleotide. These multivalent interactions result in high specificity and affinity binding that is fundamental in genetics and gene expression across all organisms, as well as antisense oligonucleotide therapeutics and DNA nanotechnology.

Interestingly, within the field of DNA nanotechnology, a tertiary level of multivalency in DNA hybridization has emerged with the ability to further strengthen and tune binding affinity. This tertiary level of multivalency in DNA hybridization occurs when multiple oligonucleotides that are anchored on a scaffold bind a target simultaneously. Tertiary multivalent nucleic acid interactions have been explored between two one-dimensional scaffolds bound together by identical pairs of oligonucleotides.[5] The affinity of this homomultivalent (homoMV) interaction was found to increase linearly with the number of oligonucleotides displayed. Moreover, many copies of an oligonucleotide have been arranged on a particle or nanomaterial surface to multivalently bind an oligocoated surface or another oligocoated particle.[6−10] These homoMV tertiary multivalent interactions, as well as those found in some DNA origami structures, display a heightened affinity, allowing for useful applications in sensing, DNA motors, and supramolecular assembly.[11] However, many desirable applications, including gene regulation and mRNA sensing, require binding with high affinity to single-stranded polynucleotides hundreds of bases long and with a nonrepeating sequence, which homoMV

Received: February 9, 2020
Published: April 27, 2020

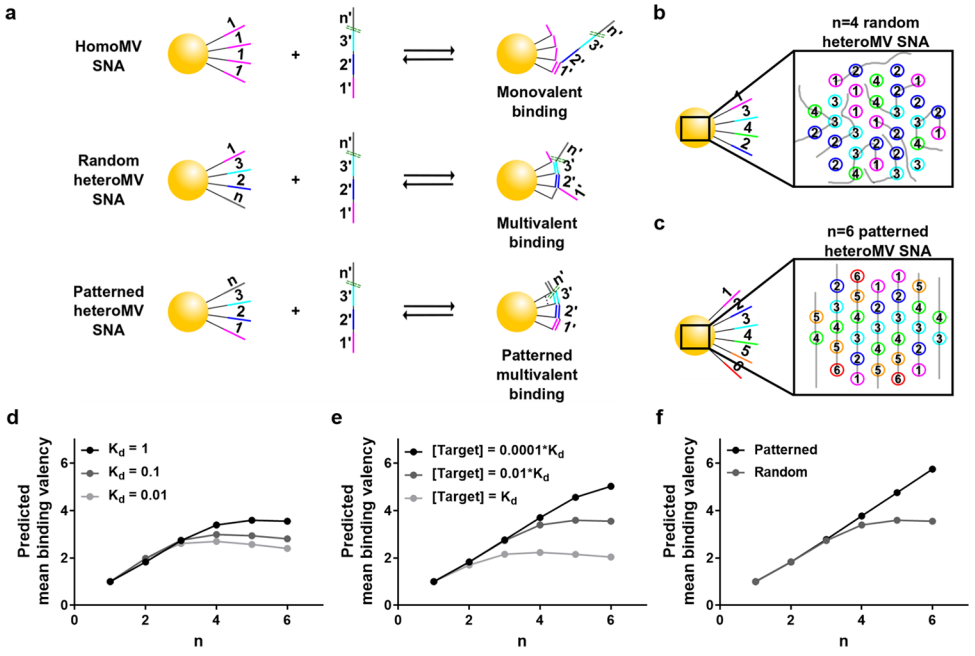

Figure 1. Binding of target to random and patterned heteroMV SNAs. (a) Schematic illustration depicting homoMV SNAs, random heteroMV SNAs, and patterned heteroMV SNAs binding a target. (b) Top-down perspective of the target binding an $n = 4$ heteroMV SNA with random segment arrangement (numbered circles = binding segments, gray line = target). (c) Top-down perspective of the target binding an idealized $n = 6$ heteroMV SNA with patterned segment arrangement. (d) Modeling results showing the impact of individual segment binding affinity on the predicted binding valency for random heteroMV SNAs. (e) Modeling results showing the impact of target concentration on the predicted binding valency for random heteroMV SNAs assuming $K_d = 1$ (arbitrary units). (f) Modeling results showing the impact of segment spatial patterning on the predicted binding valency assuming $K_d = 1$ and [Target] = $0.01*K_d$.

structures are unable to bind multivalently. To multivalently bind such targets, it is necessary to engineer heteromultivalent (heteroMV) structures that present a series of unique oligonucleotide sequences, each able to bind a distinct stretch of the target. Currently, little is known about the multivalent interaction between nanostructures presenting heteroMV DNA and a nucleic acid target. Therefore, the goal of this work is to investigate and quantify heteroMV nucleic acid binding to provide insight into designing nanostructures that bind single-stranded polynucleotides with improved affinity.

One prominent DNA-functionalized nanostructure that can be used as a model system to explore multivalent binding interactions is the spherical nucleic acid (SNA).[12,13] SNAs are typically comprised of many copies of an oligonucleotide arranged around a spherical core, such as a gold nanoparticle. SNAs presenting a highly dense layer of oligonucleotides are able to bind monovalently to their target sequence with enhanced affinity that can be more than 2 orders of magnitude greater than that of linear sequences (Figure 1a).[14−16] This high-affinity interaction has allowed SNAs' utility in many applications, most notably RNA sensing-based diagnostics and gene regulation.[17−20] Herein, we adapt the SNA platform to display a heteroMV layer of short oligos attached to a gold nanoparticle. We hypothesize that heteroMV SNAs can form tertiary multivalent interactions with a single-stranded nucleic acid target (Figure 1a). Recognizing the importance of ligand positioning in multivalency,[1,21] we tested a second hypothesis that spatial patterning of the DNA oligos on the particle surface can lead to further enhancement in target affinity. This prediction was studied by developing a new facile strategy to create spatially positioned oligonucleotides, where the target nucleic acid templates the molecular deposition of oligos on the nanoparticle surface (Figure 1a).

Specifically, we investigate heteroMV SNAs comprised of up to six unique oligo sequences designed to bind a ∼90 nt DNA target. Through modeling and experiments, we reveal that the binding valency of heteroMV SNAs with randomly anchored oligos increases with the inclusion of each additional unique oligosequence (n) but eventually decreases due to the random arrangement. Moreover, we determined the thermodynamic parameters governing multivalent binding and found that random heteromultivalency leads to an increase in affinity of up to ∼50 orders of magnitude compared to the corresponding homoMV SNA as a result of increasing the enthalpic benefits from binding. Next, we show that spatial patterning of the oligos on heteroMV SNAs results in a further ∼15 order-of-magnitude enhancement in the affinity of binding relative to heteroMV SNAs with random oligo positioning. Overall, the incorporation of heteromultivalency and spatial patterning into the SNA platform offers a general and simple approach for exploring and fine-tuning the multivalent binding affinity of DNA-functionalized nanostructures, thus improving their diagnostic and therapeutic potential and utility in DNA nanotechnology.

RESULTS

Modeling Binding of Random and Patterned heteroMV SNAs. A mathematical model was first developed in order to predict the effective strength of an interaction between a target and a heteroMV SNA that is randomly arranged (Figure 1b) or spatially patterned (Figure 1c). Briefly, assuming a random arrangement of oligos with n unique sequences (sequence x, $x + 1$, ..., $n - 1$, n) on the AuNP surface, the probability of sequence x being located next to sequence $x + 1$, which is next to $x + 2$, etc., was calculated

https://dx.doi.org/10.1021/jacs.0c01568
J. Am. Chem. Soc. XXXX, XXX, XXX−XXX

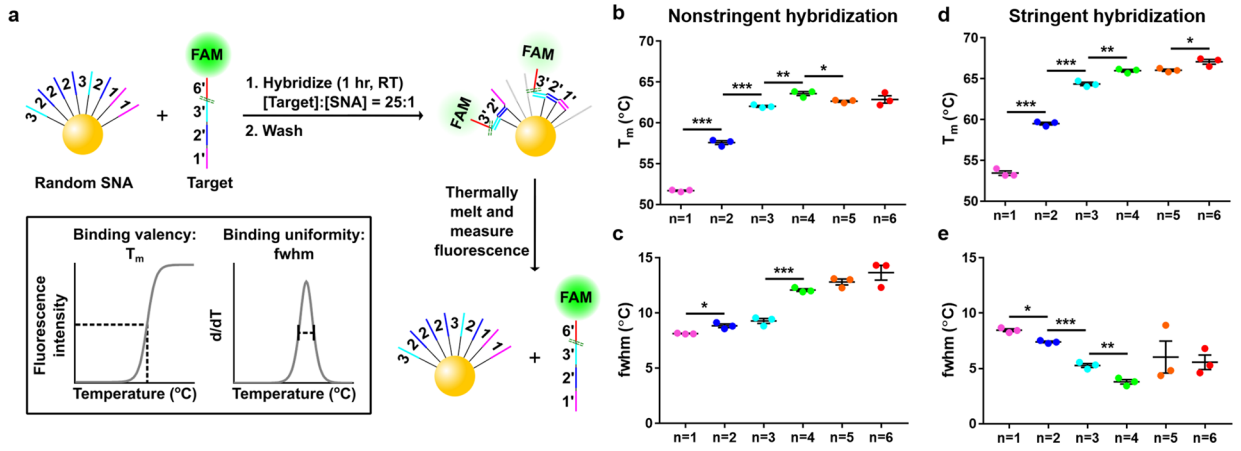

Figure 2. Effect of random heteromultivalency on binding valency and binding uniformity. (a) Schematic illustration describing the melting experiment where excess FAM-labeled target was hybridized to random n = 1−6 SNAs and fluorescence was measured as the complex was thermally melted. Inset illustrates how the melting temperature (T_m) and the full width at half-maximum (fwhm) were calculated. (b and c) Impact of increasing n on T_m (b) and fwhm (c) after hybridizing target to SNA in nonstringent buffer (1 × PBS). (d and e) Impact of increasing n on T_m (d) and fwhm (e) after hybridizing target to SNA in stringent buffer (0.1 × SSC, 0.2% Tween20). Both sets of melting curves were measured in 4 × SSC, 0.2% Tween20 buffer. Error bars represent standard error of the mean. Values from sequential groups were compared using unpaired student t tests (*P < 0.05; **P < 0.01; ***P < 0.001). No statistical differences were observed between unmarked sequential groups.

mathematically (Figure 1b). Then using Langmuir adsorption-type kinetics, the predicted mean binding valency, or average number of segments bound to a single target, was used as a proxy to estimate the strength of binding (see Methods for a detailed description). This was obtained after varying n and the K_d of the interaction between a single segment and its complementary region on the target. Significantly, the results of the model predict that as n increases, the mean binding valency will increase, plateau around n = 4, and then decrease as the probability of sequence x being neighbored by $x - 1$ or $x + 1$ decreases with increasing n (Figure 1d). Therefore, the model suggests that the probability of a random heteroMV SNA forming a maximum binding valency interaction drops as n increases. However, the model also predicts that the binding valency, as well as the value of n that leads to maximum binding valency, can be enhanced by decreasing the affinity of each segment (Figure 1d). This is because weak or labile segments allow for extensive sampling of conformational space to avoid trapping at kinetic intermediates that do not maximize binding. Alternatively, the model further reveals that decreasing the concentration of the target sequence in solution will yield higher valency binding as the probability of a target binding to a sequential series of segments (x, $x + 1$, etc.) increases (Figure 1e and Figure S1). The impact of spatial patterning on heteroMV SNA multivalent binding was also predicted by assuming each sequence x is located next to $x - 1$ and $x + 1$ (Figure 1c). The modeling results show that spatial patterning offers minimal advantage over random SNAs when n is low. However, as n increases, spatial patterning leads to higher mean binding valency compared to random heteroMV SNAs (Figure 1f). Overall, the results of the mathematical model show that a random orientation of segments will form the most efficient multivalent interaction with shorter, less stable segments or when hybridization is performed in stringent conditions (low salt, low target concentration, presence of surfactant), whereas the effects of spatial patterning will be most impactful when there are more unique segments (higher values of n).

Design and Melting Curve Analysis for Random heteroMV SNAs. To test the predictions of the modeling, six oligonucleotides (segments 1−6) between 12 and 15 nucleotides (nt) in length with similar melting temperatures were designed to bind sequentially along a 91 nucleotide DNA target based on a region of an mRNA transcript (Figure S2). To offer additional flexibility, a 2 nt spacer region was included between each segment's binding location on the target sequence, resulting in the formation of single-stranded gaps in the binding complex (see Figure S2 for further detail). Additionally, segments 1−6 each contain a T10 polynucleotide linker terminated with a thiol group at the 5′ end to allow conjugation to a ∼13 nm AuNP core. A series of SNAs were then synthesized with increasing number of distinct sequences (n) using the salt-aging method, beginning with a traditional homoMV SNA containing only segment 1 (n = 1 SNA) and ending with a heteroMV SNA incubated with equimolar concentrations of segments 1−6 (n = 6 SNA). The total number of oligos per AuNP for n = 1 and 6 SNAs was measured to be 162 ± 11 and 168 ± 6, respectively (Figure S3).

In order to determine if heteroMV SNAs form efficient multivalent interactions with the target sequence, melting curves were measured for the SNA−target complex. First, n = 1−6 SNAs were incubated for 1 h with a 25-fold excess of the target sequence labeled with FAM in 1 × PBS (Figure 2a). Following hybridization, unbound targets were removed through washing, and the samples were heated to 80 °C. As the SNA:target complex was heated, the fluorescence increased due to dehybridization and subsequent dequenching of the FAM-tagged target as the efficiency of the nanosurface energy transfer (NSET) decreased.[22] From the melting curves we determined the melting temperature (T_m), the full width at half-maximum (fwhm) of the transition, and maximum fluorescence intensity following melting. As n increased, the T_m increased by up to ∼12 °C, suggesting that multiple segments were able to bind the target simultaneously (Figure 2b). However, when n > 4 a drop in T_m was observed, supporting the predicted limitations of random heteroMV SNAs (Figure 1f). Note that one would not normally see a decrease in T_m as the duplex lengthens for conventional linear oligonucleotides. Furthermore, the fwhm of the first derivative plots of each

https://dx.doi.org/10.1021/jacs.0c01568
J. Am. Chem. Soc. XXXX, XXX, XXX−XXX

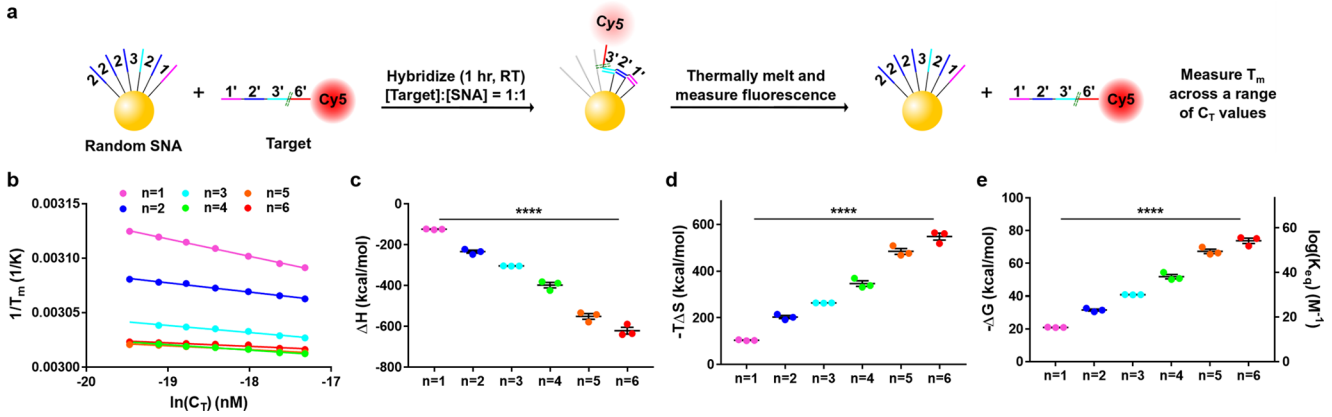

Figure 3. Effect of random heteromultivalency on thermodynamics and affinity. (a) Schematic illustration describing the experiment to obtain thermodynamic parameters and affinity values. Random n = 1−6 SNAs were bound to Cy5-labeled target in 1 × SSC, 0.2% Tween20 and the T_m was measured across a range of [SNA + target] (C_T) values. (b) Linear van't Hoff plots from which thermodynamic values were extracted. (c−e) ΔH (c), $-T\Delta S$ (d), and $-\Delta G$ and log(K_{eq}) (e) values of random n = 1−6 SNAs binding to target. Error bars represent standard error of the mean. Values were compared using one-way ANOVA (****P < 0.0001).

melting curve was determined. It was found that as n increased, the fwhm increased as well, indicating that the melting transition was less uniform (Figure 2c). This suggests that as n increased there was a wider range of binding valencies present. By incubating with a 25 molar excess of targets, we were able to also determine the number of targets bound per particle (Figure S4). Generally, as n increased, fewer targets bound each SNA, likely due to each target occupying more segments on the particle surface and the inherent reduction in maximum binding capacity as the total number of each unique oligo decreases when n increases. Next, we tested the modeling prediction that increased stringency, resulting in a lower affinity for each segment, would lead to higher valency binding. The same series of melting experiments was repeated, with the exception of performing the hybridization in a more stringent buffer, 0.1 × SSC (saline sodium citrate), 0.2% Tween20 (~15 mM Na^+). Note, the washing buffer and buffer in which the melting curves were measured are identical in the two sets of experiments. Indeed, it was observed that the T_m's for n = 1−6 SNAs increased by up to ~4 °C when hybridization stringency increased (Figure 2d). The value of n giving the highest T_m also increased to n = 6, a similar result to that predicted with modeling (Figure 1d). The noticeable ~2 °C lower T_m for the n = 1 SNA after hybridizing in less stringent conditions is consistent with previous observations of a negative cooperativity in SNA binding as an increasing number of targets are bound to the surface.[15] Furthermore, in more stringent hybridization conditions we see reversing of the trends for binding uniformity and capacity, with n = 4 resulting in the most uniform binding and the most targets bound (Figure 2e and Figure S4).

Thermodynamics and Affinity of Random heteroMV SNA Binding. We next measured the thermodynamic binding parameters of randomly organized n = 1−6 heteroMV SNAs binding to the target. In these studies, the particles were incubated at a 1:1 ratio of SNA to target for 1 h (Figure 3a). The concentration of SNA was varied from 1.75 to 15 nM, and the T_m for the complex was measured as the Cy5-labeled target was thermally dehybridized (Figure S5 and Table S1). For each SNA, ~20 thermal melting curves were used to populate the van't Hoff plot showing ln(C_T) versus $1/T_m$ (Figure 3b). Note that C_T is the sum of the SNA and target concentrations. The following equation was then applied, using 1.986 × 10^{-3} kcal K^{-1} mol^{-1} for the gas constant R, to calculate the ΔH and ΔS of binding (Table S2)

$$\frac{1}{T_m} = \frac{R}{\Delta H} \ln C_T + \frac{\Delta S - R \ln 4}{\Delta H}$$

From these values, the ΔG of binding was then derived.[15] First, consistent with the melting studies shown in Figure 2, T_m plateaued for SNAs with n > 4. The flattening slopes as n increases (Figure 3b) correspond to a more favorable enthalpy of binding (Figure 3c), suggesting that each target is binding more segments. On the other hand, the entropic cost of binding increased with increasing n as less of the target remained unbound and flexible (Figure 3d). Nonetheless, the enthalpic benefits outweighed the entropic costs, resulting in a dramatic enhancement in ΔG (~50 kcal/mol) as n increases from 1 to 6 (Figure 3e). The decrease in ΔG corresponds to a ~40 order-of-magnitude enhancement in binding affinity (K_{eq}) (Figure 3e) and a multivalent enhancement value, β (β = $K_{eq}^{multi}/K_{eq}^{mono}$), of 7 × 10^{38} as n increased from 1 to 6 (Table S3). Similar results were obtained when random heteroMV SNAs bound an identical target with no spacers between segment binding regions, with a total ~50 order-of-magnitude enhancement in avidity (Table S3). Consistent with the modeling predictions (Figure 1e), the decreased target:SNA ratio (1:1 instead of 25:1 in Figure 2) resulted in a more linear relationship between n and binding affinity, with the n = 6 heteroMV SNAs exhibiting the highest affinity. However, when the target:SNA ratio was increased to 5:1 or 10:1, the affinity of each heteroMV SNA decreased and affinity appears to saturate after n = 5 (Figure S6, Tables S4 and S5). The fwhm values also increased, suggesting that binding becomes less uniform as the target:SNA ratio increases (Figure S6).

Development and Characterization of Patterned heteroMV SNAs. Here, we hypothesized that spatial patterning of SNAs could boost target affinity compared to that of heteroMV SNAs with random oligo positioning. To test this hypothesis, we first developed a molecular printing method to create patterned heteroMV SNAs (Figure 4a). Briefly, segments 1−6 were first hybridized to a ssDNA template, identical to the no-spacer containing target sequence, forming an 81mer duplex with a "nick" located between each

https://dx.doi.org/10.1021/jacs.0c01568
J. Am. Chem. Soc. XXXX, XXX, XXX−XXX

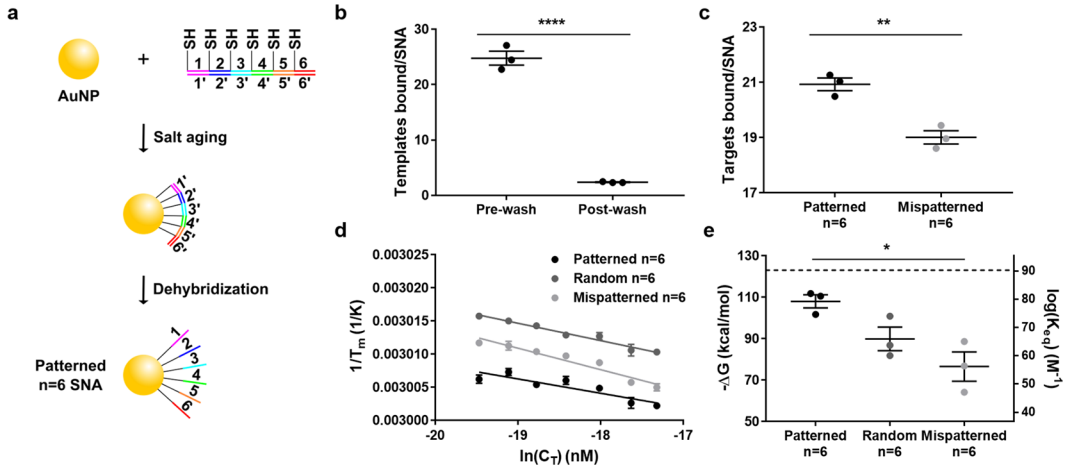

Figure 4. Characterization and binding analysis of patterned heteroMV SNAs. (a) Schematic illustration depicting the synthesis of patterned SNAs. After preannealing segments 1−6 to the template, the complex was incubated with the AuNP. Next, salt aging was performed, and then the template was dehybridized. (b) Quantifying templates bound per SNA before and after dehybridizing. (c) Targets bound per AuNP for patterned and mispatterned SNAs after high-stringency washes. (d and e) van't Hoff plots (d) and $-\Delta G$ and $\log(K_{eq})$ (e) for patterned, random, and mispatterned $n = 6$ SNAs binding the no-spacer target. Dashed line in e represents the predicted $-\Delta G$ value (123 kcal/mol) for the non-nicked 81 bp duplex binding in solution. Error bars represent standard error of the mean. Templates/targets bound values were compared using an unpaired student t test, and $-\Delta G$ and $\log(K_{eq})$ values were compared using one-way ANOVA (*$P < 0.05$; **$P < 0.01$; ****$P < 0.0001$).

segment binding region. A native PAGE gel was performed to confirm the successful binding of the six segments to the template (Figure S7). The segment/template complex was then incubated with the AuNP, forming up to six thiol linkages in a sequential array on the NP surface (as shown in Figure 4a and Figure S8). The single-strand nicks help accommodate the local curvature of the spherical nanoparticle surface.[23] Next, salt aging was performed to increase the packing density of the complex on the particle. The template was then removed by dehybridization with a series of washes in DI water at RT. After template dehybridization, segments 1−6 remain on the particle surface because of the strong thiol−gold association, with controlled position and spacing, yielding a spatially patterned heteroMV SNA with $n = 6$. Note that while we could create patterned SNAs with fewer unique segments, these structures were less desirable as the modeling suggested a maximum affinity enhancement for the $n = 6$ particles (Figure 1f).

Because patterned heteroMV SNAs have not been reported in past literature, we began by characterizing the DNA−AuNP conjugate. First, the number of complexes loaded to each particle was quantified by detecting release of a FAM-labeled template following heating (Figure S9). This melting assay revealed that ∼25 templates were bound to each SNA (Figure 4b). Next, we validated template dehybridization and found that ∼90% of templates were removed (Figure 4b). Moreover, the total number of binding ligands (segments 1−6) per particle was quantified to be ∼135 (Figure S10). This indicates that each template was bound to ∼5.5 segments, offering further evidence of successful hybridization and loading onto the particle.

Impact of Spatial Patterning on heteroMV SNA Binding. To characterize target binding by patterned heteroMV SNAs, we obtained thermal melting curves and also applied the van't Hoff relation to determine the thermodynamic binding constants. For these assays, we created mispatterned heteroMV SNAs using a template with shuffled binding regions to serve as an additional control. The mispatterned $n = 6$ SNAs are chemically identical to patterned SNAs (same total number of segments 1−6, Figure S10) except for the relative positioning of the oligos on the NP surface, allowing the role of spatial patterning to be properly elucidated. First, the two particle types were incubated with an excess amount of the no-spacer target labeled with FAM, which is identical to the template used for patterning, and washed with high-stringency buffer (0.1 × SSC, 0.2% Tween20). Thermal melting curves were then obtained by measuring the fluorescence increase while heating. While the patterned and mispatterned SNAs demonstrated a similar melting temperature (<1 °C difference), patterned SNAs were able to bind a few more targets than their mispatterned counterparts (Figure 4c and Figure S11). To more sensitively examine the effects of spatial patterning, the thermodynamics and affinity of the patterned binding interaction were quantified using the van't Hoff relation as described above and compared to the random SNAs (Figure S12, Tables S6 and S7). These experiments revealed a strong impact of oligo positioning on the binding enthalpy, as the dependence of T_m on concentration became less dramatic when going from intentionally mispatterned to random to patterned oligo positioning (Figure 4d). This enthalpic enhancement with spatial patterning is likely the result of more segments binding each target and reduced strain on the binding entities. As before, the enthalpic benefits exceeded the entropic costs, leading to a significantly more favorable binding free energy and a ∼23 order-of-magnitude enhancement in K_{eq} for patterned SNAs over mispatterned (Figure 4e). Notably, the predicted ΔG for the same duplex containing no nicks is ca. −123 kcal/mol (dashed line in Figure 4e), which is only ∼10% greater than the ΔG of the patterned SNA (−108 ± 3.2 kcal/mol) to the same target. The patterned SNAs were also able to bind the spacer-containing target with a ∼15 order-of-magnitude higher avidity relative to the mispatterned SNAs (Table S7). These results demonstrate that proper positioning of the binding ligands on the NP surface is critical for forming a highly effective multivalent interaction.

https://dx.doi.org/10.1021/jacs.0c01568
J. Am. Chem. Soc. XXXX, XXX, XXX−XXX

DISCUSSION

In this report, heteroMV SNAs were created to bind a nucleic acid target multivalently. By including multiple unique oligosequences, each complementary to a specific region of a ssDNA target, multiple oligo segments bind the target simultaneously. Aided by this multivalent binding, we observed a dramatic enhancement in the melting temperature and binding affinity relative to homoMV SNAs. Thus, the enhanced binding avidity to an oligotarget presented herein has the potential to heighten the efficacy of SNAs and other similar nanostructures in many important applications. We also identify a trade-off between maximizing the binding capacity of a nanoparticle and its binding affinity (quantity versus quality of binding). For example, we found that under stringent hybridization conditions, fewer targets bind a particle, but these few targets display a greater binding valency. In other words, under stringent conditions, the target can sample a wider range of binding geometries to overcome kinetic barriers and maximize the number of segments bound, thus reaching a thermodynamic minimum. On the basis of this conclusion, we expect that by shortening the length of each segment we can further increase the binding valency for random heteroMV SNAs.

Importantly, we demonstrate a 15 order-of-magnitude enhancement in binding affinity when six complementary oligonucleotides are spatially organized on the particle surface instead of randomly positioned. This massive enhancement is the result of a templating-based strategy to control the relative position of each oligo on the surface of the nanoparticle. To spatially pattern DNA one can use top-down or bottom-up strategies.[24−27] Bottom-up self-assembly of DNA nanostructures, such as the DNA origami technique, is clearly advantageous when the desired pattern is at the sub-100 nm length scale. Indeed, through careful template design, a variety of 2D and 3D multivalent receptors have been created to target virus capsids, proteins, and other biologically relevant molecules.[4,28,29] Our spatial patterning simply utilizes a conventional DNA oligonucleotide template and several shorter thiolated oligos. This has important advantages in terms of maximizing the yield of synthesis since DNA origami is often limited by low yields and low synthesis scale.[30] We note several reports showing the feasibility of generating a variety of DNA patterns on gold nanoparticle scaffolds.[31−33] These methods have created interesting geometries that are focused on generating nanoparticles with a discrete number of oligonucleotides with specific position and spacing. The materials have been investigated in the context of controlling material synthesis. However, the impact of spatially patterning oligonucleotides on binding affinity to a DNA target has not been characterized previously. Moreover, only by maximizing DNA density on the particle surface is it possible to achieve maximum enhancement in binding affinity.[16] We anticipate that this simple yet efficacious spatial patterning technique developed in this work can be broadly utilized in supramolecular chemistry and nanotechnology.

In conclusion, we demonstrated a simple approach to boost the affinity of DNA−nanoparticle conjugates by many orders of magnitude without making any chemical changes to its composition. Further optimization of patterned heteroMV SNAs is likely possible by considering the three-dimensional topology of the DNA duplex and positioning each segment's linker at every turn of the DNA double helix. For example, positioning the thiol group on the multivalent complex with 10−11 nucleotide intervals will likely relieve potential enthalpic strain as all of the T10 linkers should extend from the complex in the same approximate direction. However, 10−11mer segments could lower the total affinity of the heteroMV SNA for its target when compared to the longer 12−15mer segments described herein. Additionally, in this work, the binding segments are all anchored to the NP through a T10 linker. Given the importance of linker rigidity in tuning avidity, trimming the 10-nucleotide spacer may offer further enhancements in binding affinity by lowering the entropic costs of binding.[1] One limitation of the present study is that the thermodynamic parameters quantified were determined for one model target, and when this approach is applied toward designing potent binders in different biomedical or diagnostic applications, it is likely that noncanonical secondary structures may modulate the predicted avidity. To further demonstrate the general applicability of the techniques presented here, additional target sequences and the impact of the target spacer length should be investigated. A potential limitation of patterned SNAs is the labile nature of the thiol−gold bond which is highly sensitive to time, temperature, and pH.[34,35] This may be addressed by using the more stable chelating thiols anchors such as lipoic acid.[36] SNAs and other DNA-presenting nanostructures have already made their way into FDA-approved diagnostics and potential human therapies, and thus, heteromultivalent binding, both patterned and non-patterned, holds important promise for biomedical sensing and antagonism of transcripts.

ASSOCIATED CONTENT

Supporting Information

The Supporting Information is available free of charge at https://pubs.acs.org/doi/10.1021/jacs.0c01568.

Materials and Methods; modeling the impact of target concentration and surface occupancy on mean binding valency; depiction of multivalent DNA binding interaction; synthesis and characterization of heteroMV SNAs; raw melts and binding capacity determination for random heteroMV SNAs; characterization of modified oligonucleotides; impact of target:SNA ratio on random heteroMV SNAs binding thermodynamics; preparation of template/segments complex and PAGE characterization; geometric model of template/segments complex attached to the surface of AuNP; scheme, raw melts, and characterization for patterned SNAs template melting; preparation of mispatterned SNAs and determination of segment densities for patterned and mispatterned SNAs; melting characterization of patterned SNAs binding excess targets; raw melts, ΔH, and $-T\Delta S$ values for patterned, random, and mispatterned $n = 6$ heteroMV SNAs; T_m values for random heteroMV SNAs from the van't Hoff melting assay; thermodynamic values for random heteroMV SNAs; affinity values for random heteroMV SNAs; T_m values for random heteroMV SNAs from 5:1 and 10:1 target:SNA ratio van't Hoff melting assays; thermodynamic and affinity values for random heteroMV SNAs from 5:1 and 10:1 target:SNA ratio assays; T_m values for patterned SNAs from van't Hoff melting assay; thermodynamic and affinity values for patterned SNAs; supporting references (PDF)

https://dx.doi.org/10.1021/jacs.0c01568
J. Am. Chem. Soc. XXXX, XXX, XXX−XXX

AUTHOR INFORMATION

Corresponding Author

Khalid Salaita − *Department of Chemistry, Emory University, Atlanta, Georgia 30322, United States;* orcid.org/0000-0003-4138-3477; Email: k.salaita@emory.edu

Authors

Brendan R. Deal − *Department of Chemistry, Emory University, Atlanta, Georgia 30322, United States*

Rong Ma − *Department of Chemistry, Emory University, Atlanta, Georgia 30322, United States*

Victor Pui-Yan Ma − *Department of Chemistry, Emory University, Atlanta, Georgia 30322, United States*

Hanquan Su − *Department of Chemistry, Emory University, Atlanta, Georgia 30322, United States*

James T. Kindt − *Department of Chemistry, Emory University, Atlanta, Georgia 30322, United States;* orcid.org/0000-0002-9050-8144

Complete contact information is available at: https://pubs.acs.org/10.1021/jacs.0c01568

Notes

The authors declare no competing financial interest.

ACKNOWLEDGMENTS

K.S. is grateful for support from the NIH R01 HL 142866, NIH R01 GM 131099, and NIH R01 GM 124472. This project was supported in part by the Robert P. Apkarian Integrated Electron Microscopy Core and the Emory Comprehensive Glycomics Core.

REFERENCES

(1) Mammen, M.; Choi, S. K.; Whitesides, G. M. Polyvalent Interactions in Biological Systems: Implications for Design and Use of Multivalent Ligands and Inhibitors. *Angew. Chem., Int. Ed.* **1998**, *37* (20), 2754−2794.

(2) Bhatia, S.; Dimde, M.; Haag, R. Multivalent glycoconjugates as vaccines and potential drug candidates. *MedChemComm* **2014**, *5* (7), 862−878.

(3) Xu, Z.; Jia, S.; Wang, W.; Yuan, Z.; Jan Ravoo, B.; Guo, D. S. Heteromultivalent peptide recognition by co-assembly of cyclodextrin and calixarene amphiphiles enables inhibition of amyloid fibrillation. *Nat. Chem.* **2019**, *11* (1), 86−93.

(4) Kwon, P. S.; Ren, S.; Kwon, S. J.; Kizer, M. E.; Kuo, L.; Xie, M.; Zhu, D.; Zhou, F.; Zhang, F.; Kim, D.; Fraser, K.; Kramer, L. D.; Seeman, N. C.; Dordick, J. S.; Linhardt, R. J.; Chao, J.; Wang, X. Designer DNA architecture offers precise and multivalent spatial pattern-recognition for viral sensing and inhibition. *Nat. Chem.* **2020**, *12* (1), 26−35.

(5) Magdalena Estirado, E.; Aleman Garcia, M. A.; Schill, J.; Brunsveld, L. Multivalent Ultrasensitive Interfacing of Supramolecular 1D Nanoplatforms. *J. Am. Chem. Soc.* **2019**, *141* (45), 18030−18037.

(6) Lee, J. S.; Seferos, D. S.; Giljohann, D. A.; Mirkin, C. A. Thermodynamically controlled separation of polyvalent 2-nm gold nanoparticle-oligonucleotide conjugates. *J. Am. Chem. Soc.* **2008**, *130* (16), 5430−1.

(7) Liu, B.; Huang, Z.; Liu, J. Polyvalent Spherical Nucleic Acids for Universal Display of Functional DNA with Ultrahigh Stability. *Angew. Chem., Int. Ed.* **2018**, *57* (30), 9439−9442.

(8) Yehl, K.; Mugler, A.; Vivek, S.; Liu, Y.; Zhang, Y.; Fan, M.; Weeks, E. R.; Salaita, K. High-speed DNA-based rolling motors powered by RNase H. *Nat. Nanotechnol.* **2016**, *11* (2), 184−90.

(9) Blanchard, A. T.; Bazrafshan, A. S.; Yi, J.; Eisman, J. T.; Yehl, K. M.; Bian, T.; Mugler, A.; Salaita, K. Highly Polyvalent DNA Motors Generate 100+ pN of Force via Autochemophoresis. *Nano Lett.* **2019**, *19* (10), 6977−6986.

(10) Bazrafshan, A.; Meyer, T. A.; Su, H.; Brockman, J. M.; Blanchard, A. T.; Piranej, S.; Duan, Y.; Ke, Y.; Salaita, K., Tunable DNA Origami Motors Translocate Ballistically Over μm Distances at nm/s Speeds. *Angew. Chem.* **2020**. DOI: 10.1002/ange.201916281

(11) Ke, Y.; Ong, L. L.; Shih, W. M.; Yin, P. Three-dimensional structures self-assembled from DNA bricks. *Science* **2012**, *338* (6111), 1177−83.

(12) Mirkin, C. A.; Letsinger, R. L.; Mucic, R. C.; Storhoff, J. J. A DNA-based method for rationally assembling nanoparticles into macroscopic materials. *Nature* **1996**, *382*, 607−609.

(13) Cutler, J. I.; Auyeung, E.; Mirkin, C. A. Spherical nucleic acids. *J. Am. Chem. Soc.* **2012**, *134* (3), 1376−91.

(14) Lytton-Jean, A. K. R.; Mirkin, C. A. A Thermodynamic Investigation into the Binding Properties of DNA Functionalized Gold Nanoparticle Probes and Molecular Fluorophore Probes. *J. Am. Chem. Soc.* **2005**, *127*, 12754−12755.

(15) Randeria, P. S.; Jones, M. R.; Kohlstedt, K. L.; Banga, R. J.; Olvera de la Cruz, M.; Schatz, G. C.; Mirkin, C. A. What controls the hybridization thermodynamics of spherical nucleic acids? *J. Am. Chem. Soc.* **2015**, *137* (10), 3486−9.

(16) Fong, L. K.; Wang, Z.; Schatz, G. C.; Luijten, E.; Mirkin, C. A. The Role of Structural Enthalpy in Spherical Nucleic Acid Hybridization. *J. Am. Chem. Soc.* **2018**, *140* (20), 6226−6230.

(17) Giljohann, D. A.; Seferos, D. S.; Prigodich, A. E.; Patel, P. C.; Mirkin, C. A. Gene Regulation with Polyvalent siRNA−Nanoparticle Conjugates. *J. Am. Chem. Soc.* **2009**, *131*, 2072−2073.

(18) Alhasan, A. H.; Kim, D. Y.; Daniel, W. L.; Watson, E.; Meeks, J. J.; Thaxton, C. S.; Mirkin, C. A. Scanometric microRNA array profiling of prostate cancer markers using spherical nucleic acid-gold nanoparticle conjugates. *Anal. Chem.* **2012**, *84* (9), 4153−60.

(19) Seferos, D. S.; Giljohann, D. A.; Hill, H. D.; Prigodich, A. E.; Mirkin, C. A. Nano-flares: probes for transfection and mRNA detection in living cells. *J. Am. Chem. Soc.* **2007**, *129* (50), 15477−9.

(20) Rosi, N. L.; Giljohann, D. A.; Thaxton, C. S.; Lytton-Jean, A. K.; Han, M. S.; Mirkin, C. A. Oligonucleotide-modified gold nanoparticles for intracellular gene regulation. *Science* **2006**, *312* (5776), 1027−30.

(21) Kane, R. S. Thermodynamics of multivalent interactions: influence of the linker. *Langmuir* **2010**, *26* (11), 8636−40.

(22) Liu, Y.; Yehl, K.; Narui, Y.; Salaita, K. Tension sensing nanoparticles for mechano-imaging at the living/nonliving interface. *J. Am. Chem. Soc.* **2013**, *135* (14), 5320−3.

(23) Vologodskii, A.; Frank-Kamenetskii, M. D. Strong bending of the DNA double helix. *Nucleic Acids Res.* **2013**, *41* (14), 6785−92.

(24) Veneziano, R.; Ratanalert, S.; Zhang, K.; Zhang, F.; Yan, H.; Chiu, W.; Bathe, M. Designer nanoscale DNA assemblies programmed from the top down. *Science* **2016**, *352* (6293), 1534.

(25) Demers, L. M.; Ginger, D. S.; Park, S. J.; Li, Z.; Chung, S. W.; Mirkin, C. A. Direct patterning of modified oligonucleotides on metals and insulators by dip-pen nanolithography. *Science* **2002**, *296* (5574), 1836−8.

(26) Rothemund, P. W. Folding DNA to create nanoscale shapes and patterns. *Nature* **2006**, *440* (7082), 297−302.

(27) Jun, H.; Zhang, F.; Shepherd, T.; Ratanalert, S.; Qi, X.; Yan, H.; Bathe, M. Autonomously designed free-form 2D DNA origami. *Sci. Adv.* **2019**, *5* (1), eaav0655.

(28) Rinker, S.; Ke, Y.; Liu, Y.; Chhabra, R.; Yan, H. Self-assembled DNA nanostructures for distance-dependent multivalent ligand-protein binding. *Nat. Nanotechnol.* **2008**, *3* (7), 418−22.

(29) Han, X.; Jiang, Y.; Li, S.; Zhang, Y.; Ma, X.; Wu, Z.; Wu, Z.; Qi, X. Multivalent aptamer-modified tetrahedral DNA nanocage demonstrates high selectivity and safety for anti-tumor therapy. *Nanoscale* **2019**, *11* (1), 339−347.

(30) Praetorius, F.; Kick, B.; Behler, K. L.; Honemann, M. N.; Weuster-Botz, D.; Dietz, H. Biotechnological mass production of DNA origami. *Nature* **2017**, *552* (7683), 84−87.

(31) Suzuki, K.; Hosokawa, K.; Maeda, M. Controlling the number and positions of oligonucleotides on gold nanoparticle surfaces. *J. Am. Chem. Soc.* **2009**, *131* (22), 7518−9.
(32) Edwardson, T. G.; Lau, K. L.; Bousmail, D.; Serpell, C. J.; Sleiman, H. F. Transfer of molecular recognition information from DNA nanostructures to gold nanoparticles. *Nat. Chem.* **2016**, *8* (2), 162−70.
(33) Xie, N.; Liu, S.; Fang, H.; Yang, Y.; Quan, K.; Li, J.; Yang, X.; Wang, K.; Huang, J. Three-Dimensional Molecular Transfer from DNA Nanocages to Inner Gold Nanoparticle Surfaces. *ACS Nano* **2019**, *13* (4), 4174−4182.
(34) Wu, X. A.; Choi, C. H.; Zhang, C.; Hao, L.; Mirkin, C. A. Intracellular fate of spherical nucleic acid nanoparticle conjugates. *J. Am. Chem. Soc.* **2014**, *136* (21), 7726−33.
(35) Bhatt, N.; Huang, P. J.; Dave, N.; Liu, J. Dissociation and degradation of thiol-modified DNA on gold nanoparticles in aqueous and organic solvents. *Langmuir* **2011**, *27* (10), 6132−7.
(36) Dougan, J. A.; Karlsson, C.; Smith, W. E.; Graham, D. Enhanced oligonucleotide-nanoparticle conjugate stability using thioctic acid modified oligonucleotides. *Nucleic Acids Res.* **2007**, *35* (11), 3668−75.

https://dx.doi.org/10.1021/jacs.0c01568
J. Am. Chem. Soc. XXXX, XXX, XXX−XXX